chemeca CONFERENCE
30 September – 3 October 2018
Queenstown, New Zealand

Paper no. *<146>*

Chemeca 2018

30 September – 3 October 2018, Queenstown, New Zealand

Comparison of a Conjugate Heat Transfer Scheme using the Lattice Boltzmann Method

Ben W. Reynolds, Matt J. Watson and Ken R. Morison

Department of Chemical and Process Engineering, University of Canterbury, New Zealand

Abstract: The Lattice Boltzmann method (LBM) is a collision based computational fluid dynamics method used as an alternative to more traditional finite difference and finite element methods, in that LBM is built to take advantage of parallel systems. In the present case, LBM is used to model three-dimensional transient conjugate heat transfer within a box containing a solid fin. A comparison of different implementation methods for conjugate heat transfer has been carried out to determine their applicability. The geometry modelled was input as a stereolithography file, which may be generated easily by a range of packages, such as SolidWorks. From the simple box and fin geometry trialed, the solution method can easily be adapted to evaluate the suitability of structured packings for packed bed reactors, or other solid-fluid systems.

Keywords: Lattice Boltzmann method, conjugate heat transfer, transient simulations.

1 Introduction

Conjugate heat transfer is the transfer of energy between two different phases, usually a solid and a fluid. Such problems are encountered in the design of reactors, heat exchangers, or more ordinary systems such as office buildings. Across these conjugate boundaries, both conduction and convection are relevant. At the interface, both the temperature of the medium, and the heat flux passing through must be equal on each side. The proper values for these quantities can be solved either simultaneously, or through iteration. These iterations come at a computational cost, negatively impacting the performance of these solution methods, particularly when examining the dynamics of a system.

LBM was first created in 1988 [1], as an extension to the existing Lattice Gas Automata (LGA) method. In LGA, each cell of a given grid lattice can exist in one of two states; either a particle is present, or else the cell is empty. Although this treatment made the algorithm simple, it suffered greatly from statistical noise, while struggling to reach the desired level of accuracy, due to the microscopic scale to which systems needed to be discretised [1]. Replacing the Boolean states in LGA with distribution functions on the interval [0,1] based on the Boltzmann distribution resulted in a greatly more stable algorithm. With the introduction of the Bhatnager-Gross-Krook (BGK) collision operator, the basis for much of the current form of LBM was made. In this era, much effort was spent ensuring the mathematical rigour of LBM. Chen et al. [2] showed that the incompressible Navier-Stokes equations may be retrieved from LBM.

LBM consists of a grid lattice of interconnected nodes, which transfer distribution function density amongst their neighbours. Each node may only transfer to Q neighbours, including itself, in Q discrete directions, distributed amongst D dimensions. Figure 1 shows the D_3Q_{19} lattice used for the current simulations. In this setup, one central node is surrounded by 18 neighbours, to which particle population density may flow to or from at every time step. Each of these neighbours is similarly surrounded by another 18 nodes, creating a lattice. Depending on the desired speed and accuracy, many other lattice arrangements exist, with greater or fewer neighbours [3]. The D_3Q_{19} arrangement was chosen in this work as a compromise between the speed of D_3Q_{15} and the accuracy of D_3Q_{27}. The process by which population density is passed between lattice nodes along these directions is known as the collision step, and the updating of the nodes after this is the streaming step. Although this process is carried out the same across most of the domain, boundaries are a common exception, as there may be no nodes to stream to.

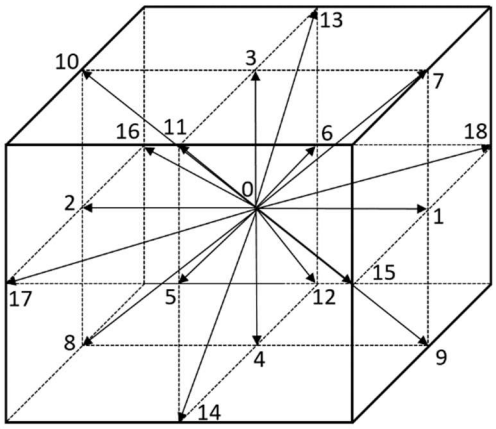

Figure 1. Orientation of the D_3Q_{19} lattice.

Macroscopic quantities are calculated in LBM by taking moments of each lattice node. The zeroth order moment, the density, is simply the sum of the lattice populations in each of the discrete directions prescribed by the aforementioned arrangements. Similarly, the first order moment is the velocity. Higher order moments can used to find the temperature and flux, provided that a large enough lattice is used that this information is preserved. Using a single, large lattice in this manner to calculate thermal effects was formerly required [4], before it was discovered that a second advection-diffusion lattice could be coupled and run in parallel [5]. Doing so allows quantities such as temperature to be determined with greater accuracy as simple zeroth order moments of the advection-diffusion lattice. Since the higher order moments are no longer required, modern schemes typically use smaller lattices such as D_3Q_{19} for each [3]. If greater computational speed is desired, the lattices do not necessarily need to match [3], allowing a yet smaller lattice to be used for thermal effects.

Many alterations can be made to the scheme to either improve computational speed or accuracy. Each adds extra layers of conceptual difficulty, as well as introducing additional parameters which may be difficult to find accurately. An example is the Multiple Relaxation Time (MRT) scheme. In this case, the simple BGK collision operator is replaced with a matrix of relaxation parameters, which must be tuned for the specific system being used, for each moment. One of the major benefits of MRT, despite this complication and extra computational difficulty, is that it allows higher Reynolds number flows to be modelled in a more accurate and stable manner than what is possible with the standard single relaxation time [6].

One of the key advantages of LBM is the ease with which it may be parallelised and run on supercomputers. The lattices used in LBM may be split up easily into smaller blocks, which can be run in parallel on appropriate machines. The meshing system is simple in LBM, allowing complex geometries to be used. These properties make modelling 3D systems in LBM less computationally demanding than by other methods [6].

Without special treatment of the boundary, conjugate heat transfer studies using LBM are limited either to the steady state, or to materials with equal values of heat capacitance. In these cases, any solids within the simulation domain are often ignored [7], as their thermal effects may not be significant in the steady state. More recently, researchers have been investigating alternative methods of treating the conjugate boundary, to enable thermally distinct materials to be modelled dynamically. These methods generally fall into one of three categories: Those with an overlapping layer of interface cells, those that alter the streaming step of the LBM algorithm, and those that apply a source term correction factor to account for the differences at the boundaries.

Works falling into the first category generally split the thermal lattice into two parts. The boundary between these parts is the layer of cells upon which the solid-fluid boundary is situated. This is a point of distinction from other methods, where the boundary is usually between nodes. Meng et al. [8] introduced a method of this form, where the lattices were allowed to interact only on the interfaces. This coupling between lattices allows for the unknown populations on the interface to be solved, thereby ensuring continuity. Imani et al. [9] built on this, incorporating both surface and volumetric heat generation terms. Although these studies were carried out in 2D only, the method was later expanded on by Imani [10] to 3D. Lu et al. [11] used an alternative iterative technique, which would ensure that continuity of temperature and flux were maintained at the boundary to some tolerance. Although the algorithm was relatively simple to implement, and conceptually easy to understand, performance issues from the iterations may exist in large 3D systems.

While altering the streaming step, often fictitious extra image and boundary nodes are introduced to aid in ensuring the continuity condition is met. Lu et al. [12] used a method where curved boundaries were approximated as stepped straight lines, directly on the centre line between nodes. Through some interpolation and extrapolation of points on either side of the boundary, the conditions at the interface were solved. Mozafari-Shamsi et al. [13] had a variation of this where a series of ghost and image points were defined, with greater freedom in placement with respect to the boundary.

Source term corrections in 3D are less common. One example is [14], where the spatial derivative of the inverse heat capacitance is multiplied by the heat flux, for a correction term. In the bulk, the term becomes zero, as the heat capacitance is constant. At boundaries, the heat capacitance changes, and a value for the correction is calculated. This method was built on by Chen et al. [15], who altered the calculation to becoming completely local for each boundary node it was applied to. Rihab et al. [16] proposed a more simple formulation for the boundary source term, in the case of heterogeneous solid media. They introduced a first order temporal derivative across the enthalpy of the boundary nodes. Chen et al. [15] noted however that this addition comes at the cost of dropping the LBM scheme to being first order accurate only, rather than the usual second order accuracy.

This paper aims to show that the numerical model developed is in agreement with those found in literature for transient conjugate heat transfer. In addition, a non-LBM method will also be compared, to ensure the results are not an artefact of LBM only. With boundaries implemented in a generalised manner, complex geometries will be able to be trialled in the future, with minimal changes to the code required.

2 Numerical Method

2.1 Geometry

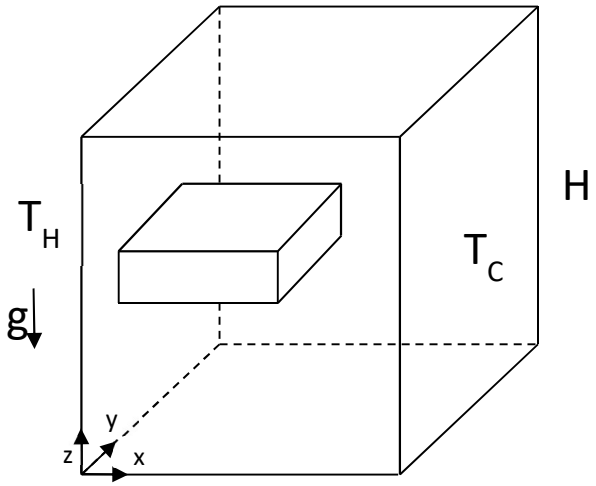

Figure 2. Finned enclosure in present study.

The finned enclosure being studied is shown in Figure 2. The left hand wall, upon which a solid fin is mounted, is set to a hot temperature, T_H, while the opposite wall is set to a cold temperature, T_C. All other outer boundaries are set to be adiabatic. Gravity is oriented in the downward, negative z axis direction. The box has sides of length *H*, upon which the fin is positioned at the centre of the y-z plane. The fin is of width $h = H/2$ in the *y* direction, length $l = H/2$ in the *x* and thickness $t = H/10$ in *z*. These ratios are preserved through the process of non-dimensionalising the system and subsequent discretising back into lattice units.

2.2 Numerical Model

The collision equation is the core of LBM, as the main driving equation advancing the system. In the present work, the double distribution function method is used, whereby one lattice, *f* tracks the density of the fluid, while a second advection diffusion lattice *g*, tracks the temperature. Equations 1 and 2 are the collision equations for the momentum and thermal lattices. e_i is the discrete velocity unit vector in each lattice direction; $\delta_x = \delta_t = 1$ are the lattice space and time steps, in lattice units; τ is the relaxation period controlling the size of the time steps; f^{eq} and g^{eq} are equilibrium distribution functions, towards which the system will relax; *F* is a body force

term acting on the fluid, in this case the Boussinesq approximation; and *Q* is a heating source term, in this case acting on the surface of the fin.

$$f_i(x + e_i\delta_t, t + \delta_t) - f_i(x,t) = -\frac{1}{\tau_v}\left[f_i(x,t) - f_i^{eq}(x,t)\right] + \delta_t F_i(x,t) \tag{1}$$

$$g_i(x + e_i\delta_t, t + \delta_t) - g_i(x,t) = -\frac{1}{\tau_g}\left[g_i(x,t) - g_i^{eq}(x,t)\right] + \left(1 - \frac{1}{2\tau_g}\right)Q_i(x,t) \tag{2}$$

A third lattice g_{si}, is used for the parts of the domain residing with the solid region. A separate lattice is used as the relaxation time of the solid differs from that of the fluid.

$$g_{si}(x + e_i\delta_t, t + \delta_t) - g_{si}(x,t) = -\frac{1}{\tau_{gs}}\left[g_{si}(x,t) - g_{si}^{eq}(x,t)\right] \tag{3}$$

Each direction of the lattice has its own weighting, depending on spatial orientation. These weightings are unique to each number of lattice directions, but are otherwise independent of the system being studied. The weightings for the D_3Q_{19} lattice are given by:

$$\omega_i = \begin{cases} \frac{1}{3} & i = 0 \\ \frac{1}{18} & i = 1-6 \\ \frac{1}{36} & i = 7-18 \end{cases} \tag{4}$$

The discrete velocity for each direction of the D_3Q_{19} lattice are as follows in Equation 5:

$$e_i = \begin{cases} 0 & i = 0 \\ (\pm1,0,0),(0,\pm1,0),(0,0,\pm1) & i = 1-6 \\ (\pm1,\pm1,0),(\pm1,0,\pm1),(0,\pm1,\pm1) & i = 7-18 \end{cases} \tag{5}$$

The equilibrium distribution functions are given by:

$$f_i^{eq} = \omega_i\rho\left[1 + \frac{e_i u}{c_s^2} + \frac{(e_i u)^2}{2c_s^4} - \frac{u^2}{2c_s^2}\right] \tag{6}$$

$$g_i^{eq} = \omega_i T\left[1 + \frac{e_i u}{c_s^2} + \frac{(e_i u)^2}{2c_s^4} - \frac{u^2}{2c_s^2}\right] \tag{7}$$

where ρ is the density of the fluid, *T* is the temperature and $c_s = 1/\sqrt{3}$ is the speed of sound in lattice units for the gas. ρ and T are macroscopic quantities which may be calculated for any cell as the zeroth order moment of each of their respective lattices, as in Equations 8-9.

$$\rho = \sum_i f_i \tag{8}$$

$$T = \sum_i g_i \tag{9}$$

The equilibrium distribution function for the solid lattice differs only in that the velocity is set to zero. With all terms containing velocity components cancelled, Equation 10 is greatly simplified:

$$g_{si}^{eq} = \omega_i T \tag{10}$$

Dynamic similarity is used to compare the current system to others. Each of the aforementioned lattices share a length scale *N*, while maintaining different time scales. For the natural convection problem being modelled, the Prandtl number *Pr*, and the Rayleigh number *Ra* are used to find the relaxation period for the fluid lattices, while the ratio of thermal conductivities fills the last free parameter, for the solid thermal lattice. The Rayleigh number is used for the present study as the system contains natural convection. For systems where a velocity must be specified, quantities such as the Reynolds number *Re*, or the Peclet number *Pe*, are more appropriate.

$$Pr = \frac{\nu_f}{\alpha_f} \tag{11}$$

$$Ra = \frac{g\beta(\mathrm{T_H} - T_C)H^3}{\alpha_f \nu_f} \tag{12}$$

For the dimensionless number calculations, ν_f is the kinematic viscosity of the fluid, α is the thermal diffusivity, g is the gravitational acceleration vector, β is the coefficient of thermal expansion and H is the characteristic length, taken as one side of the cube. For an ideal gas, β may be approximated as:

$$\beta = \frac{1}{T_0} = \frac{2}{T_C + T_H} \tag{13}$$

where T_0 is the average temperature of the domain, within which T_C and T_H are the cold and hot boundaries respectively.

The method by which a value of τ is found can vary between implementations of LBM, and depends on the particular system being studied. According to the method of Mohamad [17], for natural convection the characteristic velocity of the fluid can be found by Equation 14:

$$u_{char} = \sqrt{g\beta(T_H - T_C)H} \tag{14}$$

Provided that $u_{char} \leq 0.1$, the Mach number will be low enough that the flow is incompressible. Equations 11-14, may be used to solve Equations 15-16 for their respective values of τ.

$$\nu_f = (\tau_v - 0.5)c_s^2\delta_t \tag{15}$$

$$\alpha_f = \frac{5}{3}\left(\tau_g - 0.5\right)c_s^2\delta_t \tag{16}$$

A different method must be employed to find the thermal diffusivity of the solid. Since the thermal diffusivity of the fluid is known, and ratios are maintained regardless of dimensions, a ratio of the thermal properties of the solid to those of the fluid is created. The thermal diffusivity, α is made up of the quotient of the thermal conductivity, k, and the heat capacitance, ρc_p.

$$\alpha = \frac{k}{\rho c_p} \tag{17}$$

The ratio of thermal conductivity within the fin, to that of the fluid, controls the relaxation period of the solid thermal lattice, and hence the degree to which heat will travel through the solid at equilibrium. The heat capacitance, while having an effect on the dynamics, should have no effect on the final equilibrium values reached. The ratio of thermal conductivities between the solid and the fluid is given by Equation 18:

$$\lambda = \frac{k_s}{k_f} \tag{18}$$

The final relaxation period required for the system may then be found from Equation 19:

$$\alpha_s = \frac{5}{3}\left(\tau_{gs} - 0.5\right)c_s^2\delta_t \tag{19}$$

Usually, the Boussinesq approximation is applied by way of a force correction to the F term in Equation 1. However, Imani [10] showed that making an adjustment to the velocity used during the collision step was actually more computationally efficient and accurate than a force correction alone. As such, Equation 20 was used to account for the variations in density caused by the spatially changing temperature of the fluid.

$$u = \frac{1}{\rho}\left(\sum_{i=0}^{18} f_i e_i + \rho g\beta\left(T_F - T_{Ref}\right)\tau_v\delta_t\right) \tag{20}$$

Equation 20 was the version implemented at the collision step only. Elsewhere, the simplified version in Equation 21 was used instead. This quantity is the first order moment of the fluid lattice.

$$u = \frac{1}{\rho}\sum_i f_i e_i \tag{21}$$

Referring back to Figure 2, the wall holding the fin, and that opposite it are Dirichlet boundaries, with values of $T_H = 1$ and $T_C = 0$. All other outer walls are Neumann boundaries, through which the heat flux is set to zero. For the velocity, all surfaces are set to the no-slip condition, making the velocity zero. In LBM, each of these basic

forms of boundary are implemented as specified in [18]. Since the system is a closed box, there are no momentum entrances or exits. The system is initially set to zero velocity and temperature everywhere, with the exception of the previously stated hot wall.

In the case of conjugate boundaries, neither the Dirichlet nor the Neumann boundary are applicable, as the temperature and heat flux are not known. Instead, the continuity condition must be applied:

$$T^{+} = T^{-} \tag{22}$$

$$n\left[k\nabla T + \rho c_p u T\right]^{+} = n\left[k\nabla T + \rho c_p u T\right]^{-} \tag{23}$$

Equations 22 and 23 state that the temperature and heat flux, consisting of both conductive and convective components, on each side of the boundary must be equal, where *n* is a unit vector normal to the boundary. The conjugate boundary implemented in the current work is that used by Imani et al. [9], adapted for 3D, similar to the enactment from Imani [10]. Here, the concept of a counter-slip energy [18] is applied to find the missing populations on the fluid-solid boundary. The present work makes use of a layer of boundary cells between solid and fluid thermal lattices, upon which the boundary itself is situated, as outlined earlier.

3 Results

3.1 Nusselt number

For comparison to the work done by Imani [10], the system being studied is the finned box shown in Figure 2. Unless otherwise stated, simulations were carried out with $Pr = 0.71$, $Ra = 10^5$ and $\lambda = 10$. The finned box was created in SolidWorks to the specified dimensional ratios, before being exported as an STL file and voxelised for simulation. All simulations were run at a resolution of 121 cells in each direction in order to match the other studies being compared.

Similar to the method also used by Frederick and Moraga [19], the surface averaged Nusselt number *Nu* is calculated to both show the differences between the modes of heat transfer present at varying *Ra*, as well as give a quantitative measure of the progression of the simulation. The Nusselt number in Equation 24 will always start high for this system, decaying down over time.

$$Nu = \sum_{z=1}^{N}\sum_{y=1}^{N}\left(\frac{k_{yz}}{k_f}\frac{\Delta T_{yz}}{\Delta x_{yz}}\right) \tag{24}$$

Here, ΔT_{yz} is the change in dimensionless temperature between the cells on the hot wall, situated at $x = 1$, and those cells immediately adjacent to them on the lattice slice at $x = 2$. Δx_{yz} is the dimensionless distance between the aforementioned cells and k_{yz} is their thermal conductivity. For the fin geometry of Figure 2, the ratio k_{yz}/k_f will be equal to $\lambda = 10$ only for the solid phase cells within the fin, and is equal to unity for the fluid on the bare wall. Once the relative change in *Nu* between successive steps became small, the system was assumed to have reached a steady state.

3.2 Steady State

Figures 3 and 4 show the steady state temperatures profiles for $Ra = 10^5$ and $Ra = 10^4$ respectively, for the finned enclosure. Although reasonable agreement can be seen between the present work and that of the existing numerical data, minor differences are present. Compared with that of Imani, the current work appears to have a slightly higher velocity under the fin. This carries heat further along the length of the fin and deforms the temperature profile. A similar effect may be seen above the fin.

The expected behaviour for a closed, natural convection system is for the vertical velocity to increase from zero against the hot wall, before rotating clockwise, being cooled by the cold wall and sinking again. The introduction of the fin both introduces a medium upon which heat may extrude further into the cube, as well as deflecting the convection current previously formed. The speed and degree to which heat may travel along the fin depend on the thermal properties assigned to it. For the steady state system, only the thermal conductivity ratio is important.

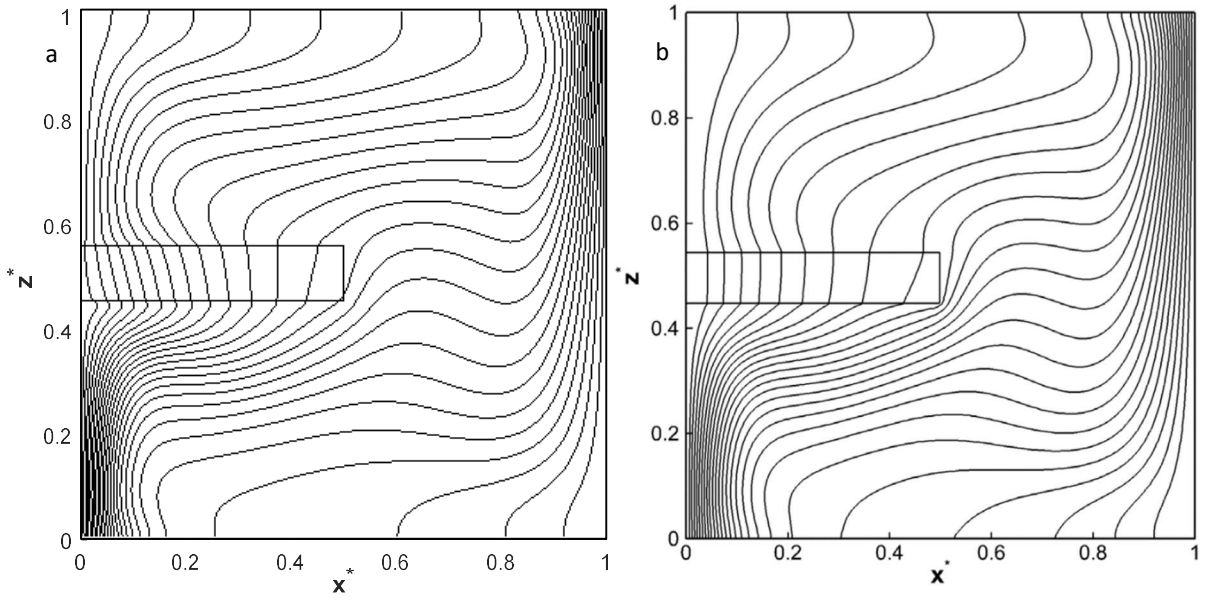

Figure 3. Temperature isotherms at steady state and $Ra = 10^5$ for (a) present work and (b) Imani [10].

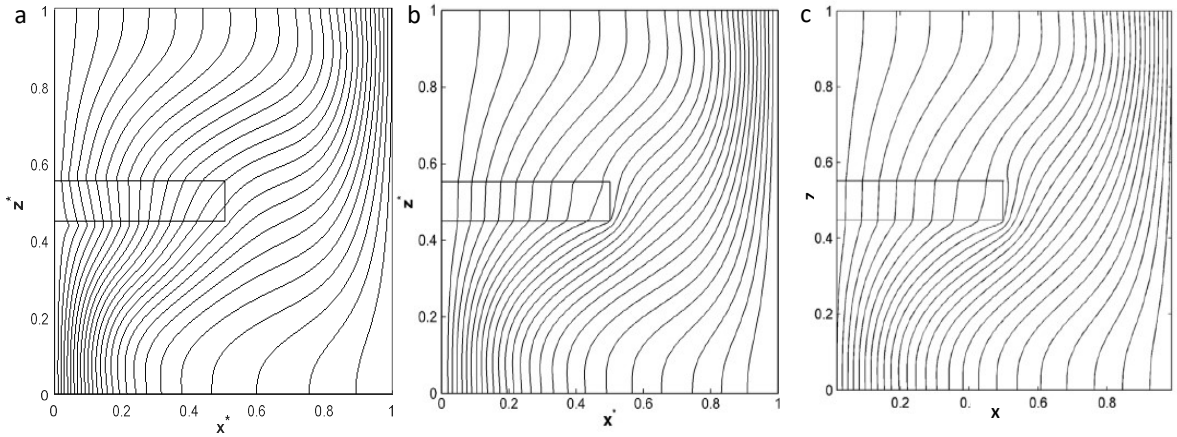

Figure 4. Temperature isotherms at steady state and $Ra = 10^4$ for (a) present work, (b) Imani [10] and (c) Frederick and Moraga [19].

At the lower Rayleigh number used in Figure 4, heat is transferred more slowly, with a lower velocity than was seen previously, due to the effects of dynamic similarity. The deformation of the isotherms under the fin are far less pronounced than they were in the previous case. Good agreement between the results may be observed in general, though the isotherms at the tip of the fin differ slightly. The work of Frederick and Moraga [19] includes a setup of the same system as that studied, solved using the finite volume method instead. Close agreement may be seen between this and the work of Imani.

3.3 Dynamics

Dynamics show greater differences due to the relatively fast changes that occur in the system at the start of the simulation. With the initial condition of $T = 0$ everywhere except the hot wall on the left, and the previously described boundary conditions, the progression of heat through the box is shown in Figure 5. All parameters remain the same as those in Figure 3, with the exception of the time at which the images were taken.

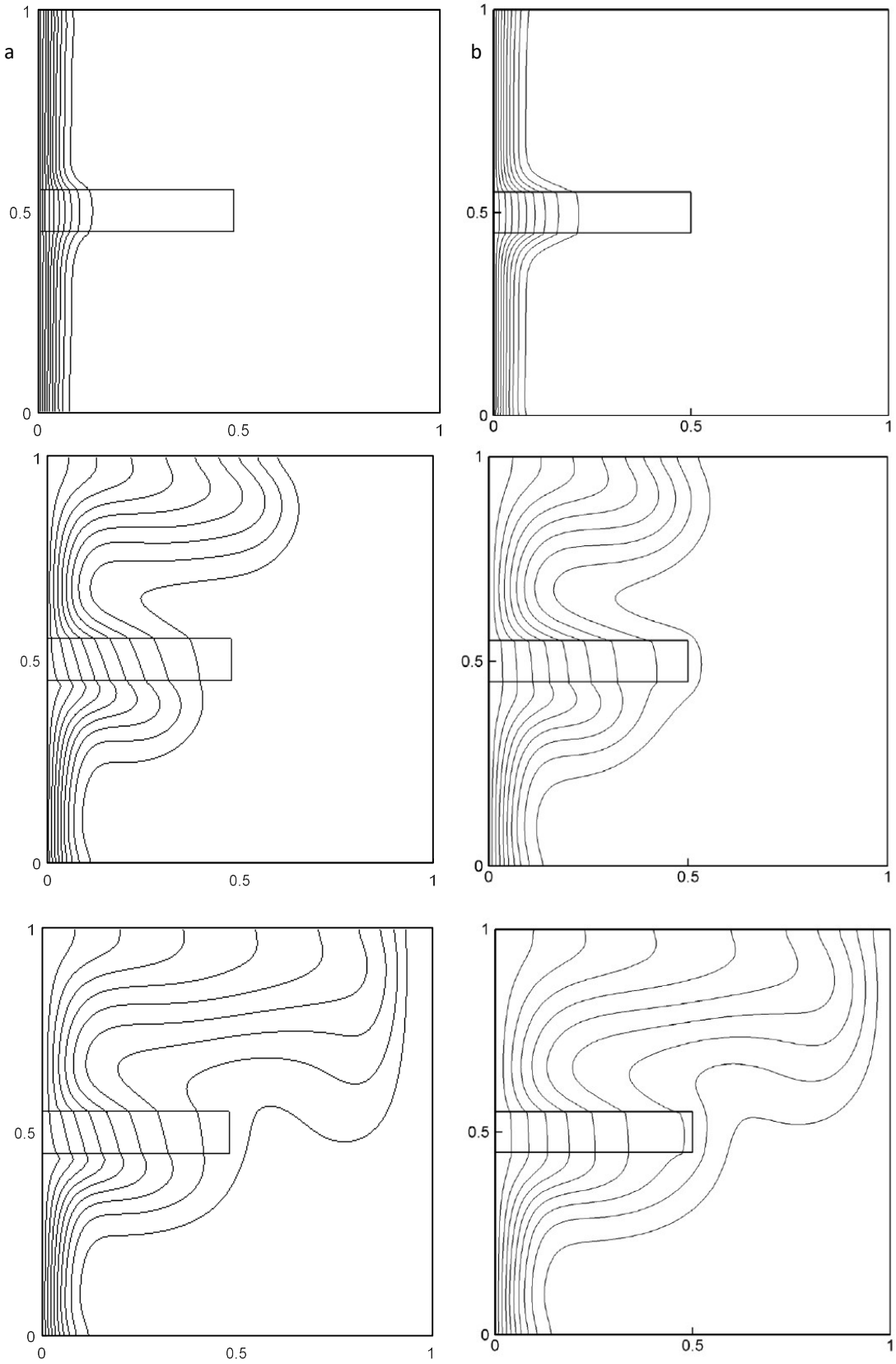

Figure 5. Dynamic temperature isotherms for (a) present work and (b) Imani [10]. Top to bottom these images are taken at $t^* = 0.0018$, $t^* = 0.0188$ and $t^* = 0.0375$ respectively.

As expected, at the beginning of the simulations in Figure 5, the temperature profile is dominated by heat conduction through the solid, due to the thermal conductivity ratio of 10. Over time, fluid begins to move as it is heated and made less dense, carrying energy with it to the other side of the box. During the early stages of the simulation, heat in the current work spreads slower, resulting in a difference of approximately one isotherm line. Later in the simulation, the present work appears to catch up somewhat, likely due to the apparently higher velocity increasing the rate of heat transfer from the wall. Over greater time, each simulation approaches a similar steady state, as in Figure 3. Although most relevant physical systems will have materials with differing heat capacitances, in this work the heat capacitance ratio between the phases has been left at unity so that works can be accurately compared.

The surface averaged Nusselt number defined earlier tracks well with those found by Imani, as shown in Figure 6. In Imani's work, the circle and delta markers are for simulations first without, and then with special treatment of the conjugate boundary, for systems with equal heat capacitance ratios. In this case, the results should be similar, as no special treatment effectively forces the heat capacitances to be equal. Although the surface average Nusselt number calculated in the present work is close to that found in the previous work for the entire time domain, a small but consistent offset is present. This offset exists as a result of the slightly higher velocities in the current work, as supported by the small differences in the temperature profiles.

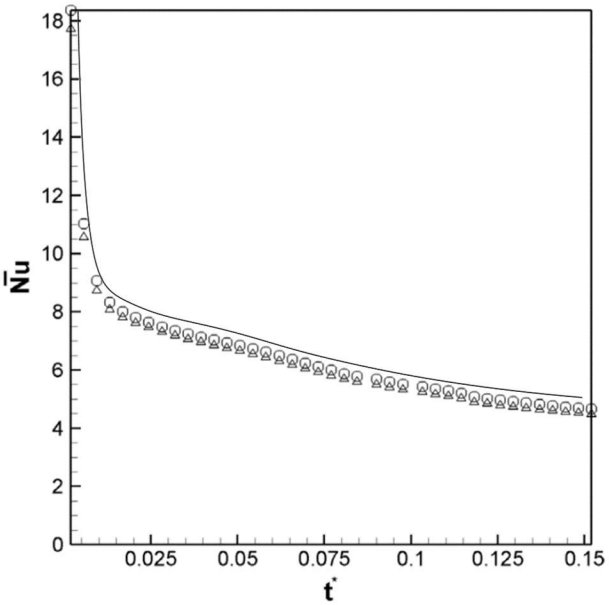

Figure 6. Hot wall Nusselt number over time for (line) present work and (O and Δ) Imani [10].

4 Conclusions

A Lattice Boltzmann model capable of accurately simulating transient conjugate heat transfer problems was created. Heat transfer characteristics were measured and compared against published research. The present work was in good agreement both with another LBM model, and one using the finite volume method.

The geometry to be simulated need only be supplied in STL format to the program at the point it is run, as most boundary conditions are applied automatically. This generality of geometry makes the model applicable for simulating a range of applications across chemical engineering without significant alterations. Although only materials with the same heat capacitance were used in the current study, this was done for the sake of comparisons against existing data. The work can easily be extended to other materials with varying heat capacitance ratios, with applications across the field of chemical engineering. Extending the model further to incorporate heat generation terms will allow reactive systems to be studied more in depth with LBM.

References

1. McNamara, G.R. and G. Zanetti, 1988. *Use of the Boltzmann-equation to simulate lattice-gas automata.* Physical Review Letters, **61**(20): p. 2332-2335.

2. Chen, H.D., S.Y. Chen, and W.H. Matthaeus, 1992. *Recovery of the Navier-Stokes equations using a lattice-gas Boltzmann method.* Physical Review A, **45**(8): p. R5339-R5342.

3. Peng, Y., C. Shu, and Y.T. Chew, 2004. *A 3D incompressible thermal lattice Boltzmann model and its application to simulate natural convection in a cubic cavity.* Journal of Computational Physics, **193**(1): p. 260-274.

4. McNamara, G.R., A.L. Garcia, and B.J. Alder, 1997. *A hydrodynamically correct thermal lattice Boltzmann model.* Journal of Statistical Physics, **87**(5-6): p. 1111-1121.

5. He, X., S. Chen, and G.D. Doolen, 1998. *A novel thermal model for the lattice Boltzmann method in incompressible limit.* Journal of Computational Physics, **146**(1): p. 282-300.

6. Wu, J.S. and Y.L. Shao, 2004. *Simulation of lid-driven cavity flows by parallel lattice Boltzmann method using multi-relaxation-time scheme.* International Journal for Numerical Methods in Fluids, **46**(9): p. 921-937.

7. Xin, F., X.F. Li, M. Xu, X.L. Huai, J. Cai, and Z.X. Guo, 2013. *Simulation of Gas Exothermic Chemical Reaction in Porous Media Reactor with Lattice Boltzmann Method.* Journal of Thermal Science, **22**(1): p. 42-47.

8. Meng, F.K., M. Wang, and Z.X. Li, 2008. *Lattice Boltzmann simulations of conjugate heat transfer in high-frequency oscillating flows.* International Journal of Heat and Fluid Flow, **29**(4): p. 1203-1210.

9. Imani, G., M. Maerefat, and K. Hooman, 2012. *Lattice Boltzmann simulation of conjugate heat transfer from multiple heated obstacles mounted in a walled parallel plate channel.* Numerical Heat Transfer Part a-Applications, **62**(10): p. 798-821.

10. Imani, G., 2017. *Three dimensional lattice Boltzmann simulation of steady and transient finned natural convection problems with evaluation of different forcing and conjugate heat transfer schemes.* Computers & Mathematics with Applications, **74**(6): p. 1362-1378.

11. Lu, J.H., H.Y. Lei, and C.S. Dai, 2017. *A lattice Boltzmann algorithm for simulating conjugate heat transfer through virtual heat capacity correction.* International Journal of Thermal Sciences, **116**: p. 22-31.

12. Lu, J.H., H.Y. Lei, and C.S. Dai, 2017. *A simple difference method for lattice Boltzmann algorithm to simulate conjugate heat transfer.* International Journal of Heat and Mass Transfer, **114**: p. 268-276.

13. Mozafari-Shamsi, M., M. Sefid, and G. Imani, 2016. *New formulation for the simulation of the conjugate heat transfer at the curved interfaces based on the ghost fluid lattice Boltzmann method.* Numerical Heat Transfer Part B-Fundamentals, **70**(6): p. 559-576.

14. Karani, H. and C. Huber, 2015. *Lattice Boltzmann formulation for conjugate heat transfer in heterogeneous media.* Physical Review E, **91**(2): p. 12.

15. Chen, S., Y.Y. Yan, and W. Gong, 2017. *A simple lattice Boltzmann model for conjugate heat transfer research.* International Journal of Heat and Mass Transfer, **107**: p. 862-870.

16. Rihab, H., N. Moudhaffar, B. Sassi, and P. Patrick, 2016. *Enthalpic lattice Boltzmann formulation for unsteady heat conduction in heterogeneous media.* International Journal of Heat and Mass Transfer, **100**: p. 728-736.

17. Mohamad, A.A., 2011, *Lattice Boltzmann Method: Fundamentals and engineering applications with computer codes*. London;New York;: Springer.

18. D'Orazio, A. and S. Succi, 2003,*Boundary conditions for thermal lattice Boltzmann simulations*, in *Computational Science - Iccs 2003, Pt I, Proceedings*, M.A.P. Sloot, et al., Editors. Springer-Verlag Berlin: Berlin. p. 977-986.

19. Frederick, R.L. and S.G. Moraga, 2007. *Three-dimensional natural convection in finned cubical enclosures.* International Journal of Heat and Fluid Flow, **28**(2): p. 289-298.